

Article

Synergistic Effects between Lignin, Cellulose and Coal in the Co-Pyrolysis Process of Coal and Cotton Stalk

Xuehe Ding, Lihua Yan, Chang Guo, Dianzeng Jia, Nannan Guo * and Luxiang Wang *

State Key Laboratory of Chemistry and Utilization of Carbon-Based Energy Resources, College of Chemistry, Xinjiang University, Urumqi 830017, China; dxh428216850@163.com (X.D.); yanlihua0516@163.com (L.Y.); y1364523303@163.com (C.G.); jdz@xju.edu.cn (D.J.)

* Correspondence: guonan067@xju.edu.cn (N.G.); wangluxiang@xju.edu.cn (L.W.)

Abstract: In this work, Qiqunahu (QQH) coal, cotton stalk, cellulose and lignin extracted from cotton stalk were selected as raw materials to study the effects of the co-pyrolysis of coal and cotton stalk. Online thermogravimetric mass spectrometry (TG-MS) was used to analyse mass loss and gas release characteristics during co-pyrolysis. The results reveal that the mixture of cotton stalk and coal can significantly enhance the reactivity of the blends and promote the formation of effective gas. The cellulose in the cotton stalk promotes the generation of H₂ and CO₂ during the co-pyrolysis of coal and cotton stalks. Lignin promotes the production of CH₄ and CO₂. Cellulose and lignin show an inhibitory effect on the precipitation of small molecular weight hydrocarbon gases during co-pyrolysis. This study provides a better understanding for the co-pyrolysis of biomass and coal.

Keywords: coal; cotton stalk; cellulose; lignin; co-pyrolysis; synergistic effects

1. Introduction

Energy demand continues to rise with the rapid development of the global economy [1,2]. Fossil fuels are a widely available energy resource, though this resource of energy production is associated with large amounts of greenhouse gas emissions, a driver of climate change [3–5]. Coal is still the largest raw material of power in China, which consumes billions of tons every year. However, as a kind of non-renewable energy, coal releases a lot of toxic gas (SO₂, NO_x, et al.) and other environmental pollutants during the combustion process. The government of China has proposed a target of becoming carbon neutral by 2060. Therefore, it is an urgent problem to cleanly and efficiently use coal resources.

As a renewable and eco-friendly energy source, biomasses are widely distributed on the Earth [6,7], which absorbs large amounts of CO₂ as it grows. Meanwhile, the carbon contained in the biomass can be liberated in the gasification process. This indicates that the entire process of biomass growth and utilization is zero emission. However, biomass has low energy density, low gasification temperature and high transportation cost [8–10], which greatly limits the large-scale utilization of biomass.

The advantages of coal and biomass separate gasification can be fully exploited with mixed coal and biomass gasification technology, which is a promising energy utilization technology with high efficiency and clean conversion [11–14]. Co-pyrolysis is the first step in the co-gasification of biomass and coal, which has considerable influence on the following reactions [15]. Therefore, studies have been carried out in this area over the past decades. Co-pyrolysis includes the devolatilization of biomass and coal to form coke, tar and gases, resulting in solid-gases and gases-tar reactions [16–18]. The high hydrogen content indicates that biomass could act as a hydrogen donor in co-pyrolysis with coal [6,19,20]. Hence, co-pyrolysis of coal and biomass can not only pave the theoretical support for greater efficiency with better utilization of biomass and coal, but also reduce the activation energy of the reaction for co-pyrolysis of coal and biomass [21,22], which



Citation: Ding, X.; Yan, L.; Guo, C.; Jia, D.; Guo, N.; Wang, L. Synergistic Effects between Lignin, Cellulose and Coal in the Co-Pyrolysis Process of Coal and Cotton Stalk. *Molecules* **2023**, *28*, 5708. <https://doi.org/10.3390/molecules28155708>

Academic Editor: Rafal M. Lukasik

Received: 28 June 2023

Revised: 21 July 2023

Accepted: 26 July 2023

Published: 28 July 2023



Copyright: © 2023 by the authors. Licensee MDPI, Basel, Switzerland. This article is an open access article distributed under the terms and conditions of the Creative Commons Attribution (CC BY) license (<https://creativecommons.org/licenses/by/4.0/>).

are conducive to industrializing and large-scale development. The whole process reduces polluting emissions and significantly improves utilization efficiency.

As the region with the most abundant coal and cotton stalk resources in China, Xinjiang has great potential in the gasification of coal and biomass. However, the mechanism of promoting or restraining effect in the co-pyrolysis process is still uncertain, and in-depth studies on co-pyrolysis are still lacking. Herein, the release behavior of small molecules during the co-pyrolysis of cotton stalk and coal were measured by the online thermogravimetric-mass spectrometer (TG-MS). The distribution of the gaseous products of cellulose, lignin, cotton stalk, QQH coal and their blend during co-pyrolysis were analyzed. This study is helpful to elucidate the interaction mechanism of coal and cotton stalk co-pyrolysis engineering, which provides the theoretical basis for large-scale industrial applications with high production efficiency. Co-pyrolysis of coal and cotton stalk can achieve dual benefits in environmental protection and economy, which provides a new direction for the practical significance for the future utilization of coal and cotton stalks.

2. Results and Discussion

2.1. Physicochemical Properties of Sample

The FT-IR spectra in Figure 1 show that the chemical structures of the four raw materials are quite different [23–25]. Compared with the biomass-derived samples, raw coal shows weaker -OH, -C-O-C-, -COOH, -CH bands and stronger C=C, C=CH bonds, indicating the glucosidic bond of biomass-derived samples and the aromatic structure of raw coal, respectively. The FT-IR spectra of cellulose and lignin showed strong intensity of absorption peak at 3100–3700 cm^{-1} , suggesting abundant surface hydroxyl groups. Moreover, the highest peaks of intensity of the out-of-plane deformation mode of -CH at 610 cm^{-1} and 870 cm^{-1} reveal the hydrogen in cotton stalks mainly comes from cellulose. Differently from cellulose, lignin and raw coal possess two absorption peaks at 3000–2800 cm^{-1} and an absorption peak at 1380 cm^{-1} . This is mainly attributed to the abundant methylene in CL and rich -O-CH₃ in the lignin and raw coal. The band at 1760 cm^{-1} caused by C=O stretching vibrations and the band at 1600 cm^{-1} derived from C=C vibration of lignin are much stronger than those of cellulose, suggesting the lactonic, carboxylic or anhydride, and aromatic ring groups in the cotton stalk mainly come from lignin. The highest peak at about 1400 cm^{-1} of raw coal suggests that the oxygen-containing functional groups of raw coal are mainly composed of phenolic hydroxyl groups.

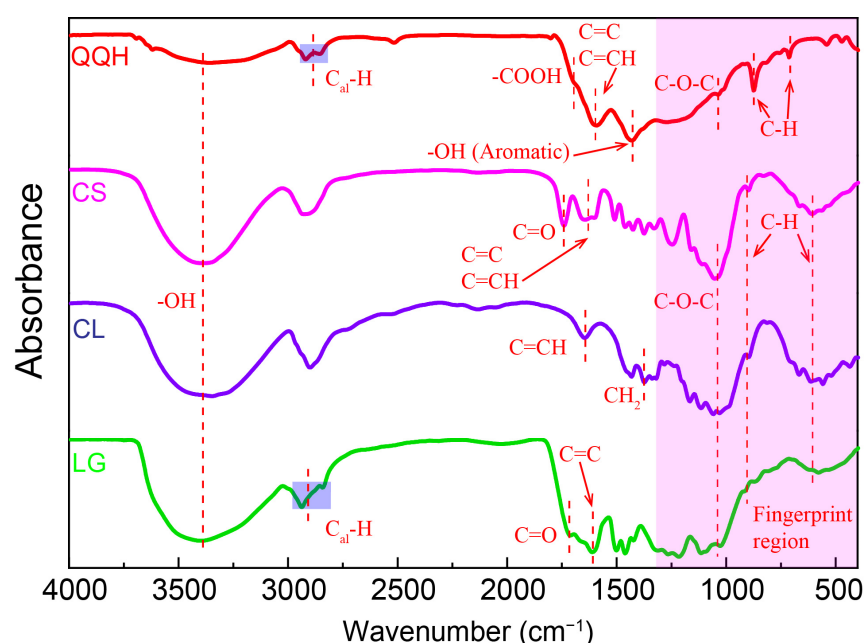


Figure 1. FT-IR spectra of four samples.

2.2. Thermal Behavior Analysis of Sample

Figure 2 shows the TG and DTG curves of QQH, CS, CL, LG and their blends at a heating rate of 20 °C/min under an Ar atmosphere. As seen in the TG curves (Figure 2a–c), the whole pyrolysis is divided into three main stages. There is little weight loss in the first stage before 200 °C, which was caused by the evaporation of adsorbed water. The weight loss in the second stage is mainly derived from the thermal decomposition of the sample in the temperature range from 200–600 °C, with the peak approximately at 380–520 °C. The weight loss rate of CS and CL is 84.59% and 90.98% in the second stage, which are almost three times than the 20.18% and 24.10% of QQH coal and LG, respectively. This indicates that CS and CL release a lot of volatile gases during the pyrolysis process. Moreover, the pyrolysis process of CS and CL has been almost completed in the second stage. The pyrolysis temperature range of the third stage is range from 680–1000 °C. The weight loss peak of QQH appears in the temperature range between 715 °C and 900 °C. On the one hand, the relatively stable aromatic ring structure in coal occurs fracture reaction in this stage. On the other hand, the minerals in coal decompose at a high temperature, such as calcium carbonate (CaCO_3). Figure 2d shows the DTG curves of all the samples. Compared to the CS, CL and LG, the initial pyrolysis temperature of the QQH coal is delayed, suggesting high temperatures are needed to disrupt the stable structure of raw coal. The addition of CS and CL make the weight loss peaks in the DTG curves of blends shift downward and increase the weight loss rate by 20.32% and 19.02% in the second stage. The blending of CL or CS with QQH can not only widen the devolatilization interval, but also increase the reactivity and the weight loss of QQH coal in the second stage. In contrast to the CL and CS, the TG and DTG curves of LG and coal blend have little obvious change with the original curves, indicating that the main reason for promoting coal pyrolysis is cellulose components in biomass precursors. By comparing the experimental curve and the calculated curve in Figure 2, the weight loss of the experimental curve is lower than that of the calculated curve, indicating the synergistic effect of coal and biomass during the co-pyrolysis process.

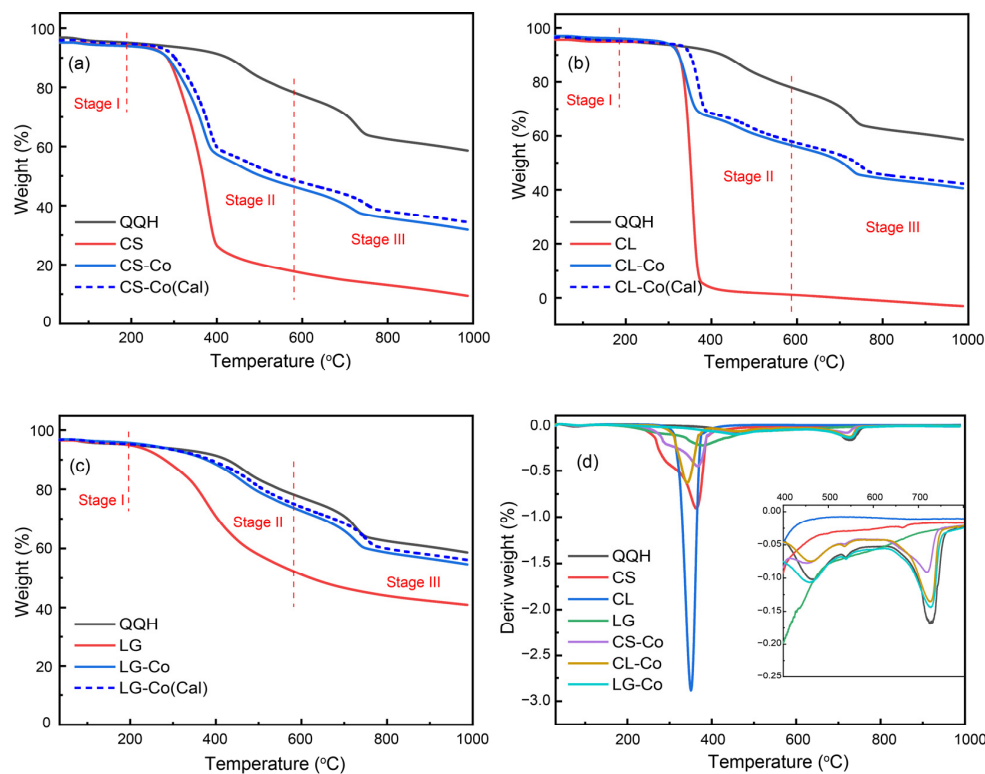


Figure 2. TG and DTG curves of sample pyrolysis: (a–c) TG; (d) DTG.

2.3. Evolution Curve of Low Molecular Weight Gases

2.3.1. Separate Pyrolysis

The gas evolution curves during the pyrolysis of QQH, CS, CL and LG in TG-MS at a final temperature of 1000 °C are shown in Figure 3. As shown in Figure 3a, H₂O, C₂H₂, CO and C₂H₆ gases begin to be released at lower temperatures, while H₂, CH₄ and CO₂ gases are released at higher temperatures during the pyrolysis of coal. More H₂O, CO and CO₂ were produced because more oxygen-containing functional groups were present in the coal. The production of small gaseous hydrocarbons and H₂ is less. Due to the low hydrogen content in coal, the hydrocarbon generation from the adipose side chain during pyrolysis is limited. On the other hand, H₂ will participate in other reactions during pyrolysis. Hence, very little H₂ can be released during pyrolysis of coal.

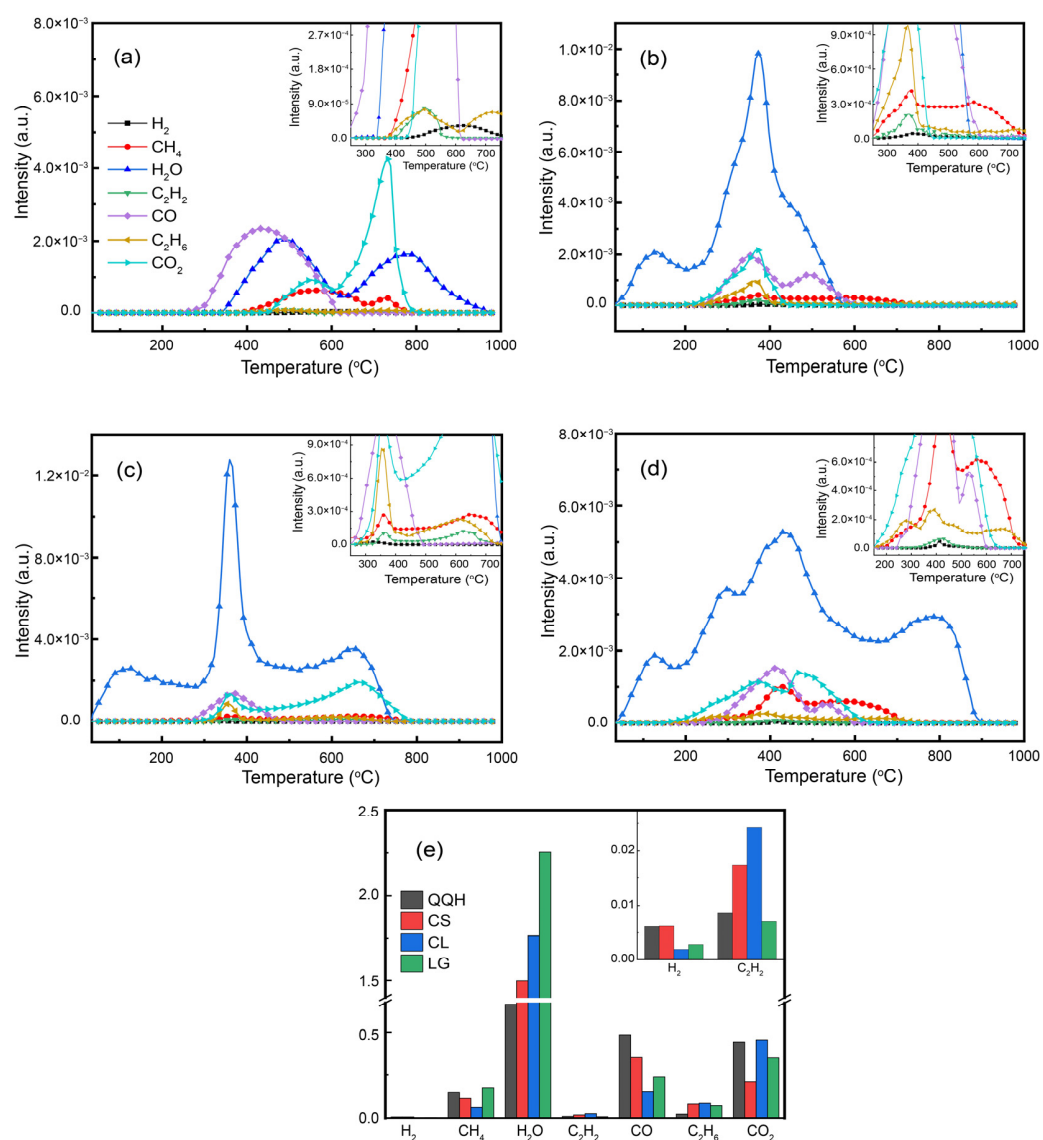


Figure 3. Gaseous evolution curves during pyrolysis: (a) QQH, (b) CS, (c) CL, (d) LG; and (e) gas yield.

As for CS, CL and LG, their structure is less stable than that of coal, so gas molecules start to release at a lower temperature during pyrolysis. As shown in Figure 3b–d, H₂O is released first, then CO, C₂H₂, C₂H₆ and CO₂, followed by H₂ and CH₄. The low bond energy of ether and hydroxyl lead to a lower break temperature (200 °C), producing abundant H₂O and CO₂. Then, the aliphatic compounds begin to crack to form gaseous hydrocarbons when the pyrolysis temperature reaches 240 °C. In addition, the produced

hydrocarbon gas will undergo secondary cracking, which results in hydrocarbon gas production near 600 °C. Then the alkyl chain starts to break at 300 °C, forming H₂ and CH₄. Figure 3e shows that the yields of H₂O, CO, CO₂ and small-molecule hydrocarbon gases during separate pyrolysis of biomass are significantly different from those of coal. For coal (QQH) and biomasses (CS, CL and LG), the composition and chemical structure are different, so the release characteristics of gas products are completely different.

2.3.2. Co-Pyrolysis of Coal and Biomass

Figure 4 shows the gas evolution curves of H₂, CH₄, H₂O, C₂H₂, CO, C₂H₆ and CO₂ in the co-pyrolysis process. Figure 4a shows that the release temperature range of sample H₂ is 430–760 °C. There are three main sources of H₂ in coal: (1) the combination of hydrogen free radicals generated after C-H bond breaking in the alkyl branch chain and the decomposition reaction of low molecular weight compounds at a low temperature [26]; (2) the dehydrogenation and condensation reactions of aromatic rings to obtain H₂ at high temperatures; and (3) the secondary cracking reactions of large hydrocarbon molecules produced at high temperatures to produce partial H₂ [27].

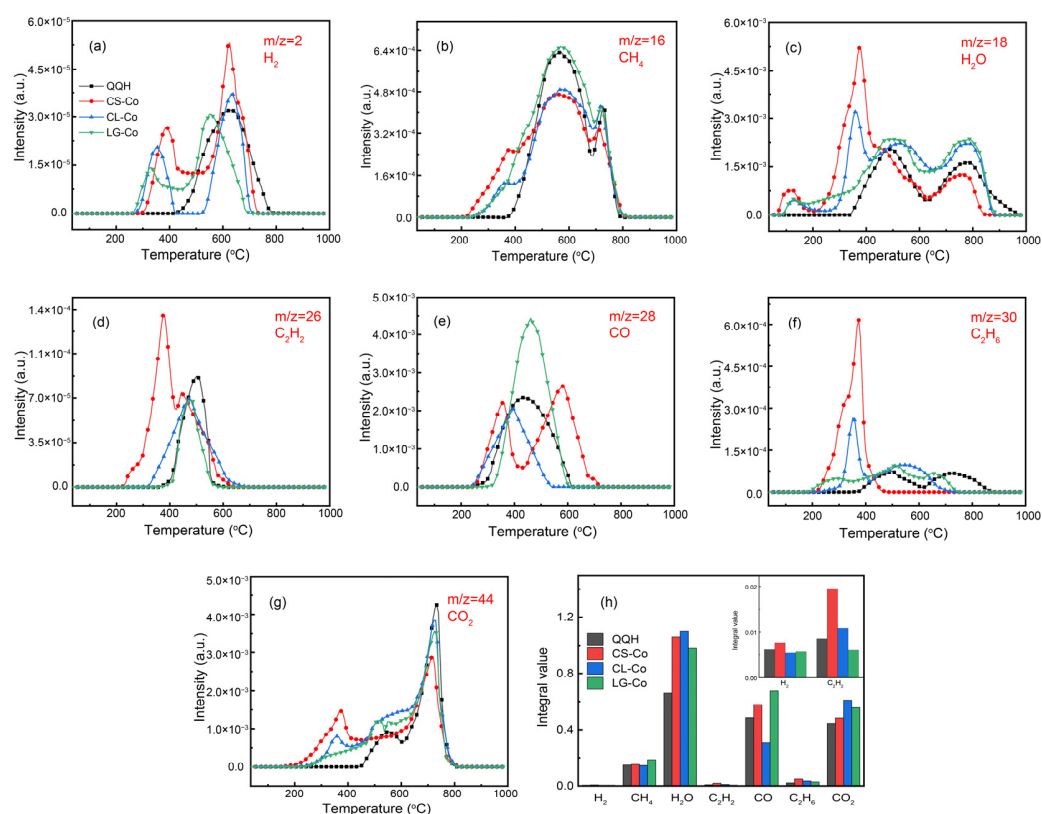


Figure 4. (a–g) Co-pyrolysis pyrolysis gas evolution curve; (h) gas yield.

Different from the pure coal, the H₂ release curves of blend show two peaks at 330–400 °C and 550–630 °C of biomass. Moreover, the H₂ produced by the pyrolysis of CS-Co has a similar evolution curve with CL-Co and LG-Co, and the peaks are superpositions of CL-Co and LG-Co. These results reveal that H₂ produced by the pyrolysis of cotton stalk is mainly derived from cellulose and lignin. The H₂ release peak of CL-Co is stronger than that of LG-Co. This mainly is because most of the hydrogen in cellulose is stored in hydroxyl and ether structures, which are subject to cleavage reactions at lower temperatures. On the other hand, the hydrogen in lignin is mostly stored in alkyl or aromatic ring structures, and less hydrogen can be released at low temperatures (330–400 °C). At high pyrolysis temperature (550–630 °C), the water produced by the pyrolysis of CL-Co is higher than that of LG-Co, which is conducive to the reactions between water and coke to produce

H₂ [28]. In addition, H₂ produced in the process of biomass pyrolysis will accelerate the cracking of long chain alkanes [29]. Combined with the peak area of H₂ release curve in Figure 4h, the addition of CS can promote H₂ production in the process of co-pyrolysis, but the increase of H₂ production is small.

The evolution curve of CH₄ during the pyrolysis of mixed samples was shown in Figure 4b. The temperature range of CH₄ release is 400–780 °C for coal, and two distinct peaks occur at 543 °C and 712 °C. At lower temperatures, methyl groups attached to ether bonds and fat chains are first to break off and become methyl radicals, which link with the hydrogen radicals to produce CH₄. The QQH coal produces more CH₄ at a moderate temperature (400–600 °C), because of the high content of fat chains and -OCH₃ in low-rank coal, as well as its easy fracture. At high temperature, the aromatic structure of coal begins to crack. The methyl group that is connected with the aromatic ring is split off by the heat to form the methyl radical, which forms CH₄ in combination with the hydrogen radical [28]. Less CH₄ is produced at higher temperatures, due to the relatively stable aromatic ring structure leading to less formation of methyl radicals.

Figure 4b shows that the release curves of CH₄ in the mixed sample with CS, CL and LG ranges from 200–800 °C. A different QQH coal, CL-Co, appears at three acromial peaks at 350 °C, 568 °C and 725 °C due to the decomposition of light aromatics at a low temperature and the hydrocarbon-branched chains at a high temperature. LG-Co shows almost a similar curve with QQH, which is attributed to the similar chemical structure between LG and coal. Moreover, the CH₄ yield of LG-Co is much more than that of CL-Co because the abundant (-O-CH₃) will undergo a demethylation reaction after temperatures higher than 400 °C. The CH₄ release pattern of CS-Co is superimposed by CL-Co and LG-Co, suggesting that the formation of CH₄ is controlled by the interaction of cellulose, lignin and coal during the co-pyrolysis process. Comparing the yield of the CH₄ in Figure 4h, the addition of lignin increased CH₄ production during co-pyrolysis, but the yield of CH₄ decreased slightly after adding CL, which may be due to the large amount of hydrogen radicals reacting with hydroxyl radicals to generate abundant H₂O during the pyrolysis of CL. Therefore, the increase of CH₄ is limited in co-pyrolysis of coal and cotton stalk under the combined action of lignin and cellulose.

Figure 4c shows the evolution curve of H₂O during the pyrolysis of mixed samples. The QQH coal began to release H₂O at 354 °C, and the acromion appeared at 461 °C and 756 °C, respectively. When the temperature exceeds 354 °C, the carbonyl groups break off and react with hydrogen to form H₂O, which shows an obvious peak at 461 °C. The peak at 756 °C is mainly attributed to the cracking of heavy hydrocarbons and the condensation of aromatic structures, which lead to the generation of H₂O. The H₂O release curves of the mixture of QQH coal and biomasses have a wide temperature range. The peaks near 100 °C are mainly caused by the release of adsorbed water from lignin and cellulose. At lower temperatures, the abundant aliphatic hydroxyl functional groups in the cellulose backbone are broken down to produce H₂O, which corresponds to the release peak at 350 °C of CL-Co. However, the apparent peak in H₂O release at 756 °C for LG-Co is due to more phenolic hydroxyl groups leaving the lignin. Comparing the yield of H₂O in Figure 4h, the H₂O yield of the blends during the co-pyrolysis is much more than that of QQH coal, which is advantageous for the gasification reaction and the water-gas conversion reaction [28]. The co-pyrolysis process of coal and CS produces more H₂O than that of the co-pyrolysis process of coal mixed with CL or LG, which may be affected by the hemicellulose, another component of the CS. In addition, the alkali and alkaline earth metals in CS and coal catalyze the ring cracking reaction to generate carboxylic acid [30], thus increasing the output of H₂O.

Figure 4d,f display the evolution curves of C₂H₂ and C₂H₆. Coal begins to release C₂H₆ at 380 °C and reaches its peak at 475 °C. The mixed samples with cellulose and lignin began to release C₂H₆ at 280 °C and 200 °C, respectively. At low temperatures, the fatty side chain breaks to produce carbon chains with lower molecular weight, and the vacant sites on the surface of these carbon chains bind hydrogen to produce C₂H₆ and C₂H₂. In the high

temperature region, it is mainly obtained by cracking of heavy hydrocarbons. In addition, C_2H_6 is dehydrogenated to produce C_2H_2 with the gradual increase of temperature [31]. Comparing the yield of C_2H_2 and C_2H_6 in Figure 4h, the yield of C_2H_2 during co-pyrolysis of coal and CS increases greatly due to the positive effect of cellulose. The production of C_2H_6 increases slightly during co-pyrolysis, which is the result of the combined action of CL and LG.

Figure 4e shows the evolution curve of CO during the pyrolysis of the mixed samples. The release of CO for coal starts near 230 °C, and an obvious peak appears at 438 °C. The pyrolysis reactivity of the different functional groups in coal is: -OH > -O- > -C-H (on the fatty chain) > -C-H (on aromatic rings) > -C=O > -COOH > -CHO. In the early stages of pyrolysis, the active aldehyde groups break and reform to produce CO, and as the temperature continues to rise, the carboxylic groups undergo decarboxylation reaction to produce CO and CO_2 . When the temperature exceeds 400 °C, the methoxy in the coal and LG begins to break and combine with hydrogen radicals to produce CH_4 and CO. Since lignin contains a large amount of methoxy, more CH_4 and CO gas is produced during co-pyrolysis of lignin and coal. Moreover, the CO release of LG-Co was significantly different from that of pure LG, suggesting that the strong interaction between LG and coal is beneficial to the release of CO during the co-pyrolysis. On the contrary, the addition of cellulose is conducive to the production of CO_2 , which reduces the yield of CO. The CO release behavior of CS-Co is similar with the pure CS, which is caused by the combined action of CL and LG. Combined with the integrated peak areas of the CO release curves in Figure 4h, the addition of biomass feedstocks results in a substantial increase in CO production during co-pyrolysis. Comparing the CO yield during co-pyrolysis after the addition of cellulose and lignin, it is inferred that the lignin in CS plays a major role in the enhanced evolution of CO during co-pyrolysis with coal.

Figure 4g shows the evolution curve of CO_2 during the pyrolysis of mixed samples. The process of CO_2 release includes volatilization and carbonization stages. CO_2 is mainly produced by the decomposition and reforming reaction of carboxyl and carbonyl groups during the volatilization phase. In the carbonization stage, the reforming reaction of C-O and carbonyl groups is the main reason for the generation of CO_2 . The temperature range of CO_2 release during the pyrolysis of coal is 420–800 °C. The acromion appeared at 537 °C and 720 °C. Carboxyl and carbonyl groups on aliphatic and aromatic groups produce CO_2 at low temperatures. At higher temperatures, CO_2 is produced by the cracking of oxygen-containing heterocyclic compounds with ether structure, quinone structure and stable structure [32].

CL-Co and LG-Co began to release CO_2 in a lower temperature region than pure QQH coal. This is induced by the low depolymerization temperature (near 200 °C) of cellulose and lignin. Only the lower strength ether bond in lignin will be C-O fracture. The acromion of CL-Co appeared at 360 °C, which was mainly caused by the breaking of carboxyl and ether bonds in CL. The acromion appeared at 512 °C in the mixed sample with lignin. On the one hand, C-C breaks are formed within alkyl chains in lignin. On the other hand, O- CH_3 in the methoxy group of lignin is fractured. Therefore, the peak value of CO_2 in the mixed sample with lignin at this stage is stronger than that of QQH coal pyrolysis alone. However, the CO_2 yield in the high temperature region (600–800 °C) of the QQH coal is higher than that of mixed samples. This mainly results from the higher oxygen content groups in the QQH coal and the unstable oxygen-containing functional groups in CS breaking down at low temperatures. Combined with the peak area of the CO_2 release curve in Figure 4h, the CO_2 yield of mixed samples during pyrolysis is higher than that of QQH coal. LG and CL play a key role in the generation of CO_2 .

2.4. Evolution Curve of Benzene and Other Aromatic Compounds

2.4.1. Separate Pyrolysis

The evolution curves of benzene, toluene and styrene during sample pyrolysis are shown in Figure 5a–c. At about 380 °C, the aromatic compounds begin to form and reach a

peak at 580 °C during the pyrolysis of coal. When the pyrolysis temperature is higher than 750 °C, no aromatic compounds are produced during coal pyrolysis. In the case of coal, the aromatic rings in the structure are connected by bridge bonds such as $-CH_2-$, $-O-$ and $-S-$. At the early stage of pyrolysis, the bridge bonds with weak stability become active and break, generating benzene ions or unsaturated structures with benzene rings, and then forming aromatic compounds through hydrogenation and other reactions. When the pyrolysis temperature is 450–650 °C, most of the bridge bonds are broken and more unsaturated structures of benzene rings are formed. When the pyrolysis temperature is higher than 650 °C, the secondary reaction of semi-coke will also produce aromatic compounds.

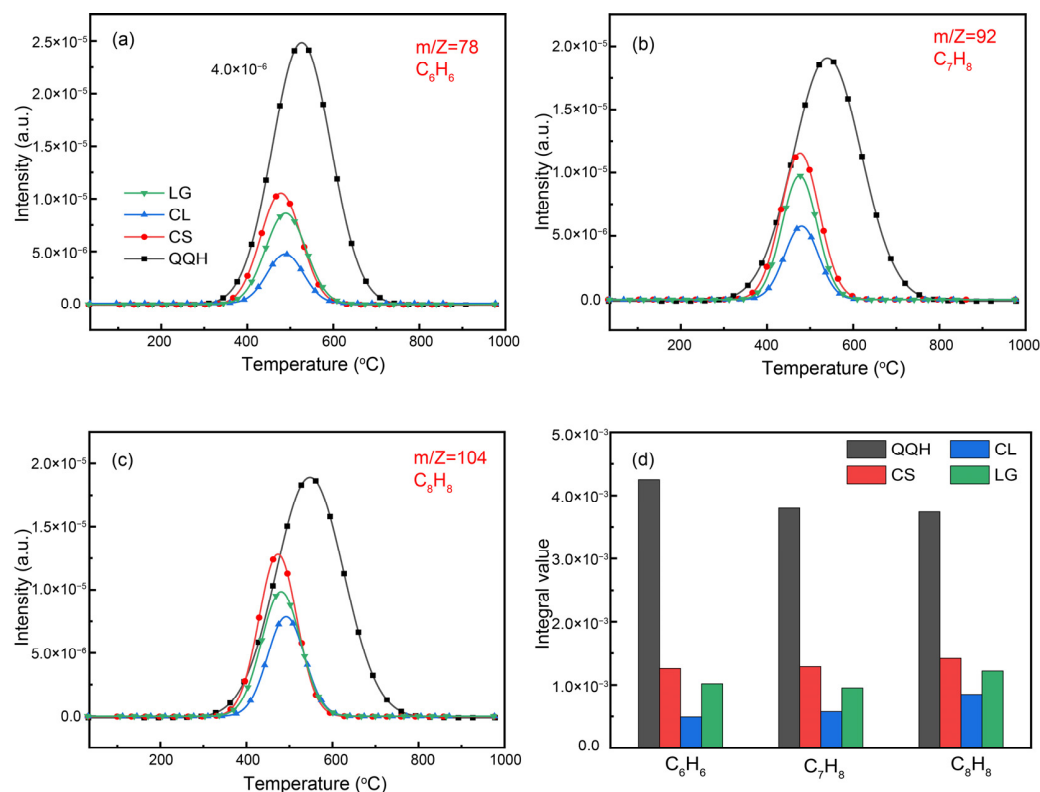


Figure 5. (a–c) Gaseous evolution curves during pyrolysis; (d) gas yield.

Compared with coal, the yield of aromatic compounds during pyrolysis of biomass samples is less (Figure 5d). This is because of the lower aromaticity of biomass, fewer aromatic rings in the structure and relatively few aromatic compounds being generated by pyrolysis. In addition, the yield of aromatic compounds in the pyrolysis of lignin is higher than that of cellulose due to the developed aromatic structure in molecular chains of lignin.

2.4.2. Co-Pyrolysis of Coal and Biomass

The evolution curve of benzene, toluene and styrene in the mixed pyrolysis process is shown in Figure 6a–c. During co-pyrolysis of cotton stalk and coal, benzene and other aromatic compounds begin to be released at 350 °C, reach a peak at 550 °C and end at 750 °C. Compared with the separate pyrolysis of coal, there is no significant change, which indicates that the synergistic effect of cotton stalk and coal co-pyrolysis has little effect on the release of benzene and other aromatic compounds. In addition, the yield of benzene and other aromatic compounds is the smallest when cellulose is mixed with coal pyrolysis (Figure 6d). This may be because the fragments formed by the cracking of cellulose combine with the aromatic structure in coal, which increases the molecular weight of the unsaturated structure-containing benzene ring formed by the fracture of bridge bonds in coal, and thus deposits semi-coke in coal coke. Hence, the released content of benzene and other aromatic compounds is significantly decreased.

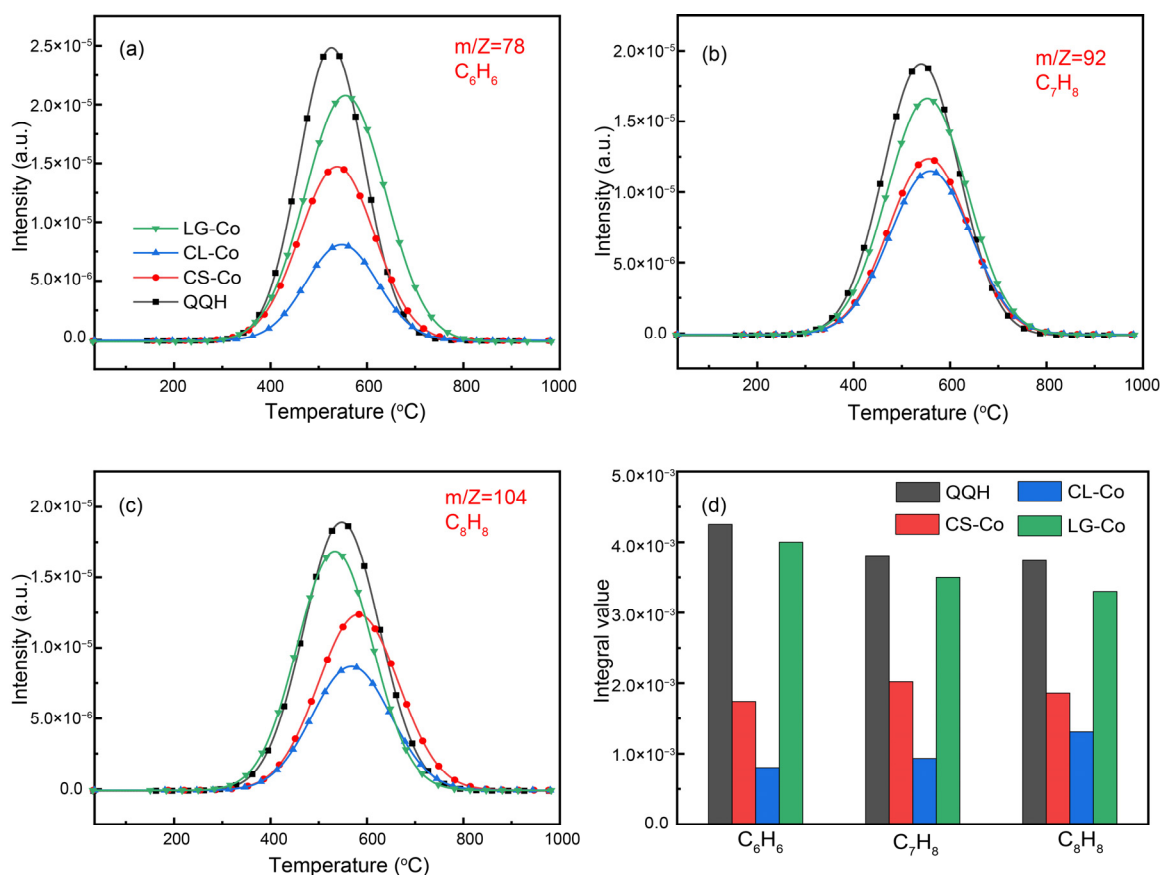


Figure 6. (a–c) Co-pyrolysis pyrolysis gas evolution curve; (d) gas yield.

2.5. Synergistic Effect

The ratio of experimental to calculated values of the yield is shown in Figure 7. As shown in Figure 7a, the synergistic effect during the co-pyrolysis of coal and cotton stalk promotes the release of H₂, CH₄, C₂H₂, CO and CO₂. The promotion of CO₂ during co-pyrolysis is similar for cellulose and lignin. The promotion effect of cellulose on H₂ during co-pyrolysis was stronger than that of lignin, and the promotion effect of lignin on CH₄ and CO was stronger than that of cellulose. In addition, CS promotes C₂H₂ during co-pyrolysis with coal, but cellulose and lignin inhibit it during co-pyrolysis with coal. This suggests that the other components of CS promote the release of C₂H₂ and the complex interactions between the components of the CS during co-pyrolysis.

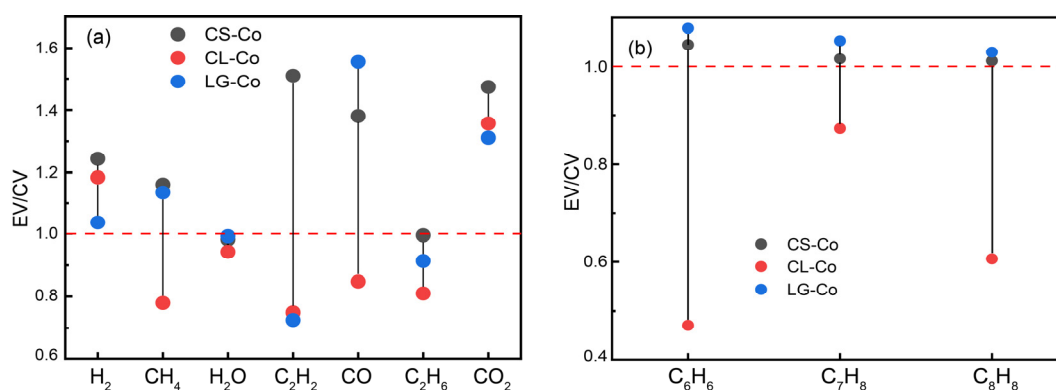


Figure 7. Ratio of experimental to calculated values. (a) low molecular weight gases; (b) benzene and other aromatic compounds.

As seen in Figure 7b, the EV/CV values of C_6H_6 , C_7H_8 and C_8H_8 are greater than 1, indicating that the synergistic effect during co-pyrolysis of coal and cotton stalks promotes the release of benzene and other aromatic compounds. Moreover, the $EV/CV > 1$ of C_6H_6 , C_7H_8 and C_8H_8 during co-pyrolysis of lignin and coal, while the $EV/CV < 1$ of C_6H_6 , C_7H_8 and C_8H_8 during co-pyrolysis of cellulose and coal. It can be determined that cellulose in cotton stalks inhibits the release of benzene and other aromatic compounds, while lignin promotes their release.

The synergistic interaction between cellulose, lignin and coal is shown in Figure 8. Abundant fragmented structures are formed at the beginning during cellulose pyrolysis [33–35]. In addition, the H^+ , H_2O and $-OCH_3$ produced by the cleavage of cellulose and lignin participate in the formation of CO and CH_4 in the coal, as in Equations (1)–(3). The large amount of water produced by cellulose at the beginning of pyrolysis facilitates the reaction in Equation (4), resulting in a reduction of CH_4 production.

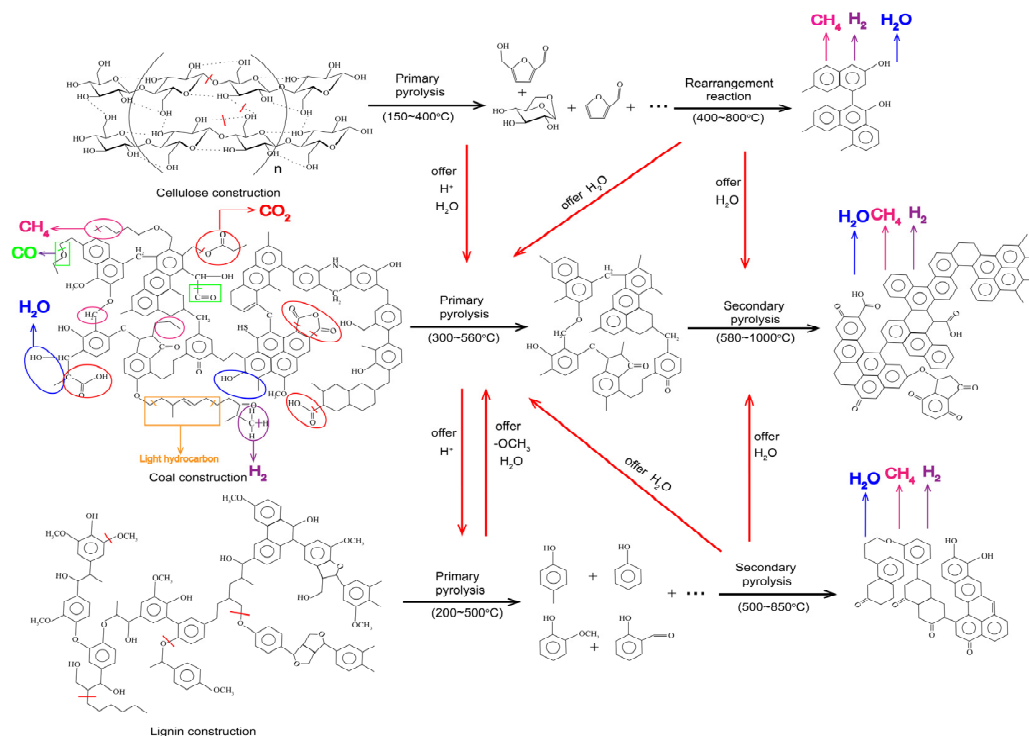
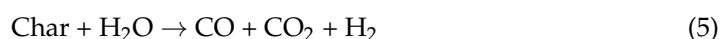
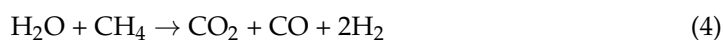


Figure 8. Diagram of the synergistic mechanism of cellulose and lignin with coal pyrolysis.

As the pyrolysis temperature gradually increases, hydrogenation of the more stable hydroxyl groups in cellulose and lignin occurs, producing water and facilitating the reaction in Equation (4). As the temperature continues to increase, the Char from the primary pyrolysis of cellulose and lignin undergoes polymerization to produce H_2O , CH_4 and

H₂. The produced H₂O will react with the char formed from the primary pyrolysis of the coal (Equation (5)), which further promotes the production of CO, CO₂ and H₂ in the high-temperature region.

3. Materials and Methods

3.1. Sample Collection and Blend Preparation

The raw materials selected for this study were cellulose, lignin, cotton stalk and Qi-quanhu bituminous coal (QQH). The QQH coal and cotton stalk are grounded to 200 mesh and 80 mesh, respectively. Cellulose and lignin were used as the biomass model components, which are extracted from cotton stalks by the nitric acid-ethanol methods [36,37] and Klason lignin method [38], respectively. According to the methods in previous works, the cotton stalk contains 20.3 wt% lignin and 37.4 wt% cellulose. In a typical process, 0.374 g cellulose, 0.203 g of lignin and 1 g of cotton stalk were mixed with 1 g QQH coal to form co-pyrolysis precursors, which were denoted as CL-Co, LG-Co and CS-Co, respectively. The proximate and ultimate analysis of cellulose, lignin and cotton stalk were performed using SDTGA5000a, SDCHN536 and SDS820. Proximate analysis and ultimate analysis of the raw materials are given in Table 1. The content of inorganic atoms in coal and cotton stalk is shown in Table 2.

Table 1. Proximate and ultimate analyses of samples.

Samples	Proximate Analysis, ad, wt%					Ultimate Analysis, d, wt%			
	M	VM	FC	A	C	H	S	O ^a	N
QQH	3.10	43.09	40.16	13.65	62.24	3.41	1.09	18.84	0.77
CS	4.30	82.39	12.52	0.79	47.37	6.41	0.05	44.87	0.51
CL	3.69	90.03	6.24	0.04	43.04	6.51	0.03	49.68	0.70
LG	3.80	53.51	39.02	3.67	59.45	5.23	5.41	25.62	0.62

Note: M—moisture; VM—volatile; FC—fixed carbon; A—ash; ad—air-dry basis; d—dry basis. ^a Calculated by difference.

Table 2. The content of inorganic atoms in samples.

Sample	mg/kg					
	K	Ca	Na	Mg	Al	Fe
QQH	612	20,314	4743	6587	1959	426
CS	902	1406	940	479	465	665

3.2. Methods

The online thermogravimetric mass spectrometer (TG-MS) was used in this experiment. Temperature rises from room temperature to 1000 °C at a rate of 20 °C/min. The test range and maximum operating temperature of the mass spectrometer are 0–300 amu and 300 °C, respectively. Ar was used as the carrier, with a flow rate of 150 mL/min.

The difference between the experimental value (EV) and calculated values (CV) of the gas yield was used to assess the synergistic interaction of QQH coal with CS, CL and LG. The calculated values were obtained by the following equation:

$$CV = EV_{\text{coal}} \times w + EV_{\text{biomass}} \times (1 - w)$$

CV represents the calculated gas yield for the blends. EV_{coal} and EV_{biomass} represent the experimental gas yield for the pyrolysis of coal and biomass samples alone, respectively. w represents the mass ratio of coal in the blends.

4. Conclusions

In summary, the addition of cotton stalks to coal promotes coal pyrolysis and leads to an increase in volatile gas production. Lignin and cellulose play different roles during the

co-pyrolysis of cotton stalks and coal. According to the online TG-MS results, the addition of cotton stalk in QQH coal can significantly enhance the reactivity of the blends and promote the formation of effective gas. Cellulose in cotton stalk contains more hydrogen and hydroxyl, which leads to more H₂ and H₂O production during co-pyrolysis. At 400 °C, the lignin in the cotton stalk began to crack and promoted the production of CH₄ and CO₂ during co-pyrolysis. The other components of the cotton stalk promote the production of C₂H₂ during co-pyrolysis, and have little effect on C₂H₆ production. In this study, the specific content of components in cotton stalks was determined, and the cellulose and lignin were co-pyrolyzed with coal according to their content in cotton stalks. The effect of the components in the cotton stalks on the co-pyrolysis was analyzed semi-quantitatively. This study has an important reference value for clean and efficient utilization of biomass and coal, and provides helpful guiding significance for determining the interaction mechanism of various mixed samples in the co-pyrolysis process.

Author Contributions: X.D.: Writing—original draft, doing experiments, data organization and software; N.G.: writing—review and editing; C.G. and L.Y.: data collation and conceptualization; L.W. and D.J.: funding acquisition, conceptualization and supervision, All authors have read and agreed to the published version of the manuscript.

Funding: This work was supported by the National Natural Science Foundation of China (22268040 and 21671166) and the Natural Science Fund for Distinguished Young Scholars of Xinjiang Uygur Autonomous Region (2021D01E09).

Institutional Review Board Statement: Not applicable.

Informed Consent Statement: Not applicable.

Data Availability Statement: Data is contained within the article.

Acknowledgments: We also thank the researchers who facilitated the completion of this study.

Conflicts of Interest: The authors declare no conflict of interest.

Sample Availability: Samples of the compounds are available from the authors.

References

1. Mehlig, D.; ApSimon, H.; Staffell, I. The impact of the UK's COVID-19 lockdowns on energy demand and emissions. *Environ. Res. Lett.* **2021**, *16*, 054037. [\[CrossRef\]](#)
2. Jess, A. What might be the energy demand and energy mix to reconcile the world's pursuit of welfare and happiness with the necessity to preserve the integrity of the biosphere? *Energy Policy* **2010**, *38*, 4663–4678. [\[CrossRef\]](#)
3. Xu, J.; Wang, J.; Du, C.; Li, S.; Liu, X. Understanding fusibility characteristics and flow properties of the biomass and biomass-coal ash samples. *Renew. Energy* **2020**, *147*, 1352–1357. [\[CrossRef\]](#)
4. Zhang, G.; Reinmüller, M.; Klinger, M.; Meyer, B. Ash melting behavior and slag infiltration into alumina refractory simulating co-gasification of coal and biomass. *Fuel* **2015**, *139*, 457–465. [\[CrossRef\]](#)
5. Du, C.; Wu, X.; Yu, G.; Song, X.; Xu, J. Investigation into the flow behavior of high-temperature ash and low-temperature ash of high calcium coal. *J. Energy Inst.* **2020**, *93*, 1951–1959. [\[CrossRef\]](#)
6. Wu, L.; Liu, J.; Xu, P.; Zhou, J.; Yang, F. Biomass hydrogen donor assisted microwave pyrolysis of low-rank pulverized coal: Optimization, product upgrade and synergistic mechanism. *Waste Manag.* **2022**, *143*, 177–185. [\[CrossRef\]](#)
7. Tauseef, M.; Ansari, A.A.; Khoja, A.H.; Naqvi, S.R.; Liaquat, R.; Nimmo, W.; Daood, S.S. Thermokinetics synergistic effects on co-pyrolysis of coal and rice husk blends for bioenergy production. *Fuel* **2022**, *318*, 123685. [\[CrossRef\]](#)
8. Herbert, G.J.; Krishnan, A.U. Quantifying environmental performance of biomass energy. *Renew. Sustain. Energy Rev.* **2016**, *59*, 292–308. [\[CrossRef\]](#)
9. Oh, K.C.; Kim, J.; Park, S.Y.; Kim, S.J.; Cho, L.H.; Lee, C.G.; Roh, J.; Kim, D.H. Development and validation of torrefaction optimization model applied element content prediction of biomass. *Energy* **2021**, *214*, 119027. [\[CrossRef\]](#)
10. Augustine, A. Spent tea waste as a biomass for co-gasification enhances the performance of semi-industrial gasifier working on groundnut shell. *Biomass Bioenergy* **2021**, *145*, 105964. [\[CrossRef\]](#)
11. Yan, L.; Cao, Y.; He, B. On the kinetic modeling of biomass/coal char co-gasification with steam. *Chem. Eng. J.* **2018**, *331*, 435–442. [\[CrossRef\]](#)
12. Kamble, A.D.; Saxena, V.K.; Chavan, P.D.; Mendhe, V.A. Co-gasification of coal and biomass an emerging clean energy technology: Status and prospects of development in Indian context. *Int. J. Min. Sci. Technol.* **2019**, *29*, 171–186. [\[CrossRef\]](#)

13. Shahabuddin, M.; Bhattacharya, S. Enhancement of performance and emission characteristics by co-gasification of biomass and coal using an entrained flow gasifier. *J. Energy Inst.* **2021**, *95*, 166–178. [[CrossRef](#)]
14. Wei, J.; Wang, M.; Xu, D.; Shi, L.; Li, B.; Bai, Y.; Yu, G.; Bao, W.; Xu, J.; Zhang, H.; et al. Migration and transformation of alkali/alkaline earth metal species during biomass and coal co-gasification: A review. *Fuel Process. Technol.* **2022**, *235*, 107376. [[CrossRef](#)]
15. Yang, Z.; Wu, Y.; Zhang, Z.; Li, H.; Li, X.; Egorov, R.I.; Strizhak, P.A.; Gao, X. Recent advances in co-thermochemical conversions of biomass with fossil fuels focusing on the synergistic effects. *Renew. Sustain. Energy Rev.* **2019**, *103*, 384–398. [[CrossRef](#)]
16. Wu, Z.; Zhang, J.; Fan, Y.; Zhang, B.; Guo, W.; Zhang, R.; Li, Y.; Yang, B. Synergistic effects from co-pyrolysis of lignocellulosic biomass with low-rank coal: A perspective based on the interaction of organic components. *Fuel* **2021**, *306*, 121648. [[CrossRef](#)]
17. Tian, B.; Wang, J.; Qiao, Y.; Huang, H.; Xu, L.; Tian, Y. Understanding the pyrolysis synergy of biomass and coal blends based on volatile release, kinetics and char structure. *Biomass Bioenergy* **2023**, *168*, 106687. [[CrossRef](#)]
18. Yuan, S.; Dai, Z.-H.; Zhou, Z.-J.; Chen, X.-L.; Yu, G.-S.; Wang, F.-C. Rapid co-pyrolysis of rice straw and a bituminous coal in a high-frequency furnace and gasification of the residual char. *Bioresour. Technol.* **2012**, *109*, 188–197. [[CrossRef](#)]
19. Zhao, S.; Yang, P.; Liu, X.; Zhang, Q.; Hu, J. Synergistic effect of mixing wheat straw and lignite in co-pyrolysis and steam co-gasification. *Bioresour. Technol.* **2020**, *302*, 122876. [[CrossRef](#)]
20. Kumar, A.; Yan, B.; Tao, J.; Li, J.; Kumari, L.; Oba, B.T.; Aborisade, M.A.; Chen, G. Influence of waste plastic on pyrolysis of low-lipid microalgae: A study on thermokinetics, behaviors, evolved gas characteristics, and products distribution. *Renew. Energy* **2022**, *185*, 416–430. [[CrossRef](#)]
21. Hong, D.; Li, P.; Si, T.; Guo, X. ReaxFF simulations of the synergistic effect mechanisms during co-pyrolysis of coal and polyethylene/polystyrene. *Energy* **2021**, *218*, 119553. [[CrossRef](#)]
22. Lu, K.-M.; Lee, W.-J.; Chen, W.-H.; Lin, T.-C. Thermogravimetric analysis and kinetics of co-pyrolysis of raw/torrefied wood and coal blends. *Appl. Energy* **2013**, *105*, 57–65. [[CrossRef](#)]
23. Mishra, R.K.; Mohanty, K. Characterization of non-edible lignocellulosic biomass in terms of their candidacy towards alternative renewable fuels. *Biomass-Convert. Biorefin.* **2018**, *8*, 799–812. [[CrossRef](#)]
24. Chen, D.; Zhou, J.; Zhang, Q. Effects of Torrefaction on the Pyrolysis Behavior and Bio-Oil Properties of Rice Husk by Using TG-FTIR and Py-GC/MS. *Energy Fuels* **2014**, *28*, 5857–5863. [[CrossRef](#)]
25. Daffalla, S.B.; Mukhtar, H.; Shaharun, M.S. Preparation and characterization of rice husk adsorbents for phenol removal from aqueous systems. *PLoS ONE* **2020**, *15*, e0243540. [[CrossRef](#)] [[PubMed](#)]
26. Li, Y.; Huang, S.; Wu, Y.; Wu, S.; Gao, J. The roles of the low molecular weight compounds in the low-temperature pyrolysis of low-rank coal. *J. Energy Inst.* **2019**, *92*, 203–209. [[CrossRef](#)]
27. Meng, A.; Zhou, H.; Qin, L.; Zhang, Y.; Li, Q. Quantitative and kinetic TG-FTIR investigation on three kinds of biomass pyrolysis. *J. Anal. Appl. Pyrolysis* **2013**, *104*, 28–37. [[CrossRef](#)]
28. Li, S.; Li, J.; Chen, H.; Xu, J. Understanding the release behavior of biomass model components and coal in the co-pyrolysis process. *J. Energy Inst.* **2022**, *101*, 122–130. [[CrossRef](#)]
29. Wang, J.; Du, J.; Chang, L.; Xie, K. Study on the structure and pyrolysis characteristics of Chinese western coals. *Fuel Process. Technol.* **2010**, *91*, 430–433. [[CrossRef](#)]
30. Saynik, P.B.; Moholkar, V.S. Influence of different salts of alkali and alkaline earth metals on the pyrolysis of *Prosopis juliflora*. *Biofuels Bioprod. Biorefin.* **2022**, *16*, 1038–1049. [[CrossRef](#)]
31. Xiong, X.; Miao, Y.; Lu, X.; Tan, H.; Rahman, Z.U.; Li, P. C1~C2 hydrocarbons generation and mutual conversion behavior in coal pyrolysis process. *Fuel* **2022**, *308*, 121929. [[CrossRef](#)]
32. Zhao, Y.; Hu, H.; Jin, L.; He, X.; Zhu, S. Pyrolysis Behavior of Macerals from Weakly Reductive Coals. *Energy Fuels* **2010**, *24*, 6314–6320. [[CrossRef](#)]
33. Chen, X.; Che, Q.; Li, S.; Liu, Z.; Yang, H.; Chen, Y.; Wang, X.; Shao, J.; Chen, H. Recent developments in lignocellulosic biomass catalytic fast pyrolysis: Strategies for the optimization of bio-oil quality and yield. *Fuel Process. Technol.* **2019**, *196*, 106180. [[CrossRef](#)]
34. Usino, D.O.; Supriyanto; Ylittervo, P.; Pettersson, A.; Richards, T. Influence of temperature and time on initial pyrolysis of cellulose and xylan. *J. Anal. Appl. Pyrolysis* **2020**, *147*, 104782. [[CrossRef](#)]
35. Yang, H.; Li, S.; Liu, B.; Chen, Y.; Xiao, J.; Dong, Z.; Gong, M.; Chen, H. Hemicellulose pyrolysis mechanism based on functional group evolutions by two-dimensional perturbation correlation infrared spectroscopy. *Fuel* **2020**, *267*, 117302. [[CrossRef](#)]
36. Malucelli, L.C.; Lacerda, L.G.; Dziedzic, M.; Filho, M.A.D.S.C. Preparation, properties and future perspectives of nanocrystals from agro-industrial residues: A review of recent research. *Rev. Environ. Sci. Bio/Technol.* **2017**, *16*, 131–145. [[CrossRef](#)]
37. Kalpana, V.; Perarasu, V. Analysis on cellulose extraction from hybrid biomass for improved crystallinity. *J. Mol. Struct.* **2020**, *1217*, 128350. [[CrossRef](#)]
38. Horst, D.J.; Behainne, J.J.R.; Júnior, P.P.D.A.; Kovaleski, J.L. An experimental comparison of lignin yield from the Klason and Willstatter extraction methods. *Energy Sustain. Dev.* **2014**, *23*, 78–84. [[CrossRef](#)]

Disclaimer/Publisher's Note: The statements, opinions and data contained in all publications are solely those of the individual author(s) and contributor(s) and not of MDPI and/or the editor(s). MDPI and/or the editor(s) disclaim responsibility for any injury to people or property resulting from any ideas, methods, instructions or products referred to in the content.